

Spin-density fluctuations and the fluctuation-dissipation theorem in 3d ferromagnetic metals

A. L. Wysocki,^{1,*} V. N. Valmispild,^{2,3} A. Kutepov,^{1,†} S. Sharma,⁴ J. K Dewhurst,⁴ E. K. U. Gross,⁴ A. I. Lichtenstein,^{2,3} and V. P. Antropov¹

¹*Ames Laboratory, Ames, IA 50011, USA*

²*Institute of Theoretical Physics, University of Hamburg, 20355 Hamburg, Germany*

³*The Hamburg Centre for Ultrafast Imaging, Luruper Chaussee 149, 22761 Hamburg, Germany*

⁴*Max Planck Institute of Microstructure Physics, Weinberg 2, D-06120 Halle, Germany*

(Dated: December 23, 2019)

Spatial and time scales of spin density fluctuations (SDF) as well as the fluctuation-dissipation theorem (FDT) were analyzed in 3d ferromagnets using *ab initio* linear response calculations of complete wavevector and energy dependence of the dynamic spin susceptibility tensor. We demonstrate that SDF are spread continuously over the entire Brillouin zone and while majority of them reside within the 3d bandwidth, a significant amount comes from much higher energies. A justification of adiabatic approximation in spin dynamics is provided. FDT is shown to have two main constituents: a minor low-energy spin wave contribution and a much larger high-energy component from local SDF. The obtained universal dependence of the on-site spin correlator (SC) and the related effective fluctuating moment on the 3d band population is further discussed.

I. INTRODUCTION

The physics of SDF^{1,2} in metallic magnets is very rich and complex. SDF determine the magnetic excitation spectrum and play an important role in the magnetic dynamics. In addition, they can strongly affect numerous static magnetic and nonmagnetic properties at zero and finite temperatures.^{3,4} SDF can be especially important near phase transitions points where they can stabilize new ground states.⁵

The key quantity characterizing SDF in metals is SC which represents the on-site spin density correlation function (see, e.g., Ref. 2). In order to obtain SC, one needs to evaluate FDT⁶ by integrating the imaginary part of the dynamic spin susceptibility over all wavevectors and energies. Such integration is, however, a highly nontrivial task which makes reliable calculations of FDT in real materials very difficult.

For instance, experimentally, SDF are traditionally studied using the neutron scattering technique. This method may be used to obtain the imaginary part of the dynamic spin susceptibility for certain points in Brillouin zone (BZ) when energies are below $\sim 0.3-0.4$ eV.⁷ While from this information FDT has been evaluated for many systems,³ such estimates are not very accurate due to small number of wavevectors and limited energy range used in the calculations. In addition, despite the clear itinerant nature of magnetic metals, in most studies the experimental results have been compared with the conclusions of a localized spin model (Heisenberg). Independently, fast and ultrafast spin dynamical experiments also detect the presence of SDF at very different frequency ranges.⁸ However, those studies are usually not related, and so far, no consistent experimental mea-

surements of the full SDF spectra in a wide energy range have been performed.

Theoretically, SDF in real materials can be explored from first principles using linear response technique based on density functional theory⁹⁻¹² or many-body perturbation methods.^{13,14} However, these calculations addressed only neutron scattering experiments and considered only limited energy and wavevector ranges. This was also related to the insufficient basis set that could not describe high energy excitations. Consequently, proper evaluation of FDT for magnetic metals is currently missing in the literature.

In addition to linear response studies of SDF, numerous theories including SDF in calculations of ground state or thermodynamic properties of materials were developed. These methods, however, have also been restricted to narrow bands energy scale and/or limited parts of the BZ. In particular, spin fluctuation models which were widely used to study effects of SDF in 3d ferromagnets^{3,15-19} employ long wavelength and low frequency approximations. On the other hand, DMFT²⁰ or single-site many-body perturbation theory²¹ include only pure intra-atomic SDF on a limited energy range. While the above mentioned approaches have been successful in the description of many systems, their essentially adjustable nature and uncontrollable approximations do not allow us to understand the relative roles of the different spatial or time scales of SDF in determining materials properties.

Clearly, a comprehensive study of the full structure of SDF in metallic magnets is necessary for a rigorous treatment of FDT. In addition, such analysis would provide an important insight about the scales of SDF that should be included in electronic structure calcula-

tions. We recently addressed this issue in 3d paramagnetic metals²² where it was shown that itinerant SDF are present throughout BZ and a wide energy range. Full FDT was evaluated resulting in a strong SC that was found to be determined solely by the 3d band population. For ferromagnetic metals, however, it is unclear how static magnetic moments interact with such itinerant SDF. Theories based on the localized Heisenberg model, which are very successful in magnetic insulators, are no longer applicable because of this intrinsic itinerancy. Therefore, a proper quantum-mechanical treatment is crucial in order to establish quantitative description of SDF in magnetic metals.

A primary goal of this paper is to present such analysis by using realistic electronic structure calculations. We focus on prototype 3d ferromagnets including Fe, Co (fcc), and Ni, where the degree of moment localization is changing gradually. We determine the strength and the character of such SDF as well as establish their spatial and energy scales. FDT is properly evaluated and the dependence of the results on the 3d band populations is studied.

II. METHOD

A. SDF formalism

SDF in solids are described by the imaginary part of the dynamic spin susceptibility tensor

$$\chi^{\alpha\beta}(\mathbf{r}, \mathbf{r}', \mathbf{q}, \omega) = -\frac{i}{\hbar} \sum_{\mathbf{R}} e^{-i\mathbf{q}\cdot\mathbf{R}} \times \int_0^\infty dt \langle [\hat{s}_\alpha(\mathbf{r} + \mathbf{R}, t), \hat{s}_\beta(\mathbf{r}')] \rangle e^{i(\omega+i\eta)t}. \quad (1)$$

Here, $\alpha, \beta = x, y, z, 0$ denote components of the tensor, \mathbf{r} and \mathbf{r}' are position vectors inside the crystal unit cell, \mathbf{q} is the wavevector in the Brillouin zone, ω is the frequency, \mathbf{R} is the lattice vector, $\langle \dots \rangle$ denotes the thermal and quantum-mechanical expectation value, $\eta \rightarrow 0^+$, and $\hat{s}_\alpha(\mathbf{r}, t)$ is the density operator when $\alpha = 0$, otherwise it is the α component of the spin density operator. For collinear magnetic states and in the absence of spin-orbit coupling, many of the tensor elements are zero. In particular, if one chooses the z axis along the magnetization direction (or sublattice magnetization in the case of antiferromagnets), the susceptibility tensor in the matrix notation becomes

$$\tilde{\chi} = \begin{pmatrix} \chi^{xx} & \chi^{xy} & 0 & 0 \\ -\chi^{xy} & \chi^{xx} & 0 & 0 \\ 0 & 0 & \chi^{zz} & \chi^{0z} \\ 0 & 0 & \chi^{0z} & \chi^{00} \end{pmatrix}, \quad (2)$$

where the dependence on \mathbf{r} , \mathbf{r}' , \mathbf{q} , and ω variables is not shown explicitly. It is convenient to express the transverse components (χ^{xx} and χ^{xy}) in terms of the circular susceptibilities

$$\chi^{+-} = 2(\chi^{xx} - i\chi^{xy}) \quad (3)$$

$$\chi^{-+} = 2(\chi^{xx} + i\chi^{xy}). \quad (4)$$

Note that the transverse components are decoupled from the longitudinal susceptibility (χ^{zz}). On the other hand, χ^{zz} is coupled to the density response (χ^{00}) through the spin-density susceptibility function χ^{0z} .

For SDF analysis, it is often not necessary to resolve intra-atomic fluctuations. Therefore, it is convenient to introduce the SDF spectral function for each nonequivalent atom by integrating the \mathbf{r} and \mathbf{r}' variables over the atomic sphere

$$A^{\alpha\beta}(\mathbf{q}, \omega) = -\frac{\hbar}{\pi} \int d\mathbf{r} \int d\mathbf{r}' \text{Im} \chi^{\alpha\beta}(\mathbf{r}, \mathbf{r}', \mathbf{q}, \omega). \quad (5)$$

Correspondingly, the density of on-site SDF can be defined by integrating $A^{\alpha\beta}(\mathbf{q}, \omega)$ over the BZ

$$N^{\alpha\beta}(\omega) = \frac{1}{\Omega_{\text{BZ}}} \int_{\Omega_{\text{BZ}}} d\mathbf{q} A^{\alpha\beta}(\mathbf{q}, \omega). \quad (6)$$

where Ω_{BZ} is the BZ volume. In order to better analyze the distribution of SDF in the BZ, one can also consider the partial- \mathbf{q} density of on-site SDF defined as

$$N_{\Omega_{\mathbf{q}}}^{\alpha\beta}(\omega) = \frac{1}{\Omega_{\text{BZ}}} \int_{\Omega_{\mathbf{q}}} d\mathbf{q} A^{\alpha\beta}(\mathbf{q}, \omega). \quad (7)$$

Here, the integration is over a Γ -point-centered sphere with the volume $\Omega_{\mathbf{q}}$ ($\Omega_{\mathbf{q}} < \Omega_{\text{BZ}}$). Further, we introduce the on-site number of transverse SDF $n^t(\omega)$ as well as longitudinal SDF $n^l(\omega)$,

$$n^t(\omega) = \frac{1}{2} \int_0^\omega d\omega' [N^{+-}(\omega') + N^{-+}(\omega')] \quad (8)$$

$$n^l(\omega) = \int_0^\omega d\omega' N^{zz}(\omega'). \quad (9)$$

FDT plays a crucial role in the physics of SDF since it allows to find a number of useful properties that characterize the SDF spectrum. In particular, it can be used to evaluate SC which is defined as an energy integral of the dynamic on-site spin density correlation function and is an important measure of the strength of SDF in solids. According to FDT, the transverse and longitudinal contributions to the SC are given by

$$\langle \mathbf{s}^2 \rangle^t(\omega) = \frac{1}{2} \int_0^\omega d\omega' \coth(\beta\omega'/2) \quad (10)$$

$$\times [N^{+-}(\omega') + N^{-+}(\omega')], \quad (11)$$

and

$$\langle \mathbf{s}^2 \rangle^l(\omega) = \int_0^\omega d\omega' \coth(\beta\omega'/2) N^{zz}(\omega'), \quad (12)$$

respectively. At $T=0$, SDF originate purely from the spin zero-point motion and we have $\langle \mathbf{s}^2 \rangle^{t,l}(\omega) = n^{t,l}(\omega)$. Therefore, the spin zero-point motion contribution to the SC is given by $n^{t,l}(\omega)$. SC is related to the effective fluctuating moment that is given by

$$m_{\text{eff}}(\omega) = \sqrt{(m_{\text{eff}}^t(\omega))^2 + (m_{\text{eff}}^l(\omega))^2}. \quad (13)$$

Here, transverse and longitudinal contributions to $m_{\text{eff}}(\omega)$ are given by

$$m_{\text{eff}}^{t,l}(\omega) = \frac{g\mu_B}{\hbar} \sqrt{\langle \mathbf{s}^2 \rangle^{t,l}(\omega)}, \quad (14)$$

where g is the electron g-factor and μ_B is the Bohr magneton. Note that according to the above equations, FDT for the full values ($\omega \rightarrow \infty$) of SC and effective fluctuating moment involves integrals over all ranges of \mathbf{q} 's and ω 's which makes such studies computationally demanding.

FDT can be also used to evaluate the value of the static magnetic moment. This leads to the following sum rule:

$$m_{\text{st}} \equiv g\mu_B \int d\mathbf{r} \langle \hat{s}_z(\mathbf{r}) \rangle = m_{\text{st}}(\omega \rightarrow \infty), \quad (15)$$

where the spatial integration is over the atomic sphere and

$$m_{\text{st}}(\omega) = \frac{g\mu_B}{4\hbar^2} \int_0^\omega d\omega' [N^{+-}(\omega') - N^{-+}(\omega')]. \quad (16)$$

Another useful quantity that characterizes SDF spectrum is the square of the magnetic moment deviation. This is defined as

$$\langle \delta m^2 \rangle(\omega) = m_{\text{eff}}^2(\omega) - m_{\text{st}}^2(\omega). \quad (17)$$

This quantity appears often in the spin fluctuation models where it is assumed to be energy independent. Here, we will discuss its energy dependence.

B. Dynamic susceptibility calculations

The dynamic spin susceptibility tensor was evaluated using the linear response time-dependent density functional theory within the local spin density approximation (LSDA).^{23,24} This technique has been employed for dynamic spin susceptibility calculations in a number of systems.⁹⁻¹² In this formalism, one first considers the Kohn-Sham (bare) susceptibility function given by

$$\chi_0^{\alpha\beta}(\mathbf{r}, \mathbf{r}', \mathbf{q}, \omega) = \sum_{\mathbf{k}} \sum_{n,m} \sum_{\sigma\sigma'}^{\text{BZ}} (f_{n\mathbf{k}}^\sigma - f_{m\mathbf{k}+\mathbf{q}}^{\sigma'}) \times \sigma_{\sigma\sigma'}^\alpha \sigma_{\sigma'\sigma}^\beta \frac{\psi_{n\mathbf{k}}^{\sigma*}(\mathbf{r}) \psi_{m\mathbf{k}+\mathbf{q}}^{\sigma'}(\mathbf{r}) \psi_{m\mathbf{k}+\mathbf{q}}^{\sigma'*}(\mathbf{r}') \psi_{n\mathbf{k}}^\sigma(\mathbf{r}')}{\hbar\omega + \epsilon_{n\mathbf{k}}^\sigma - \epsilon_{m\mathbf{k}+\mathbf{q}}^{\sigma'} + i\hbar\eta}, \quad (18)$$

where $\sigma_{\sigma\sigma'}^0 = \delta_{\sigma\sigma'}$ and $\sigma_{\sigma\sigma'}^{x,y,z}$ are elements of the Pauli matrices. The Kohn-Sham eigenfunctions $\psi_{n\mathbf{k}}^\sigma$ and eigenenergies $\epsilon_{n\mathbf{k}}^\sigma$ (the n , \mathbf{k} , and σ indices denote band, wavevector, and spin quantum number, respectively), are obtained from standard LSDA calculations. Finally, $f_{n\mathbf{k}}^\sigma \equiv f(\epsilon_{n\mathbf{k}}^\sigma)$ is the Fermi-Dirac distribution function.

The full (enhanced) susceptibility is then given by the Dyson-like equation

$$\chi^{\alpha\beta}(\mathbf{r}, \mathbf{r}', \mathbf{q}, \omega) = \chi_0^{\alpha\beta}(\mathbf{r}, \mathbf{r}', \mathbf{q}, \omega) + \sum_{\gamma\delta} \int d\mathbf{r}_1 d\mathbf{r}_2 \times \chi_0^{\alpha\gamma}(\mathbf{r}, \mathbf{r}_1, \mathbf{q}, \omega) f_{\text{Hxc}}^{\gamma\delta}(\mathbf{r}_1, \mathbf{r}_2, \mathbf{q}) \chi^{\delta\beta}(\mathbf{r}_2, \mathbf{r}', \mathbf{q}, \omega). \quad (19)$$

Here,

$$f_{\text{Hxc}}^{\alpha\beta}(\mathbf{r}, \mathbf{r}', \mathbf{q}) = e^2 \delta_{\alpha 0} \delta_{\beta 0} \sum_{\mathbf{R}} \frac{\exp(-i\mathbf{q} \cdot \mathbf{R})}{|\mathbf{R} + \mathbf{r} - \mathbf{r}'|} + f_{\text{xc}}^{\alpha\beta}(\mathbf{r}) \delta(\mathbf{r} - \mathbf{r}'), \quad (20)$$

where $f_{\text{xc}}^{\alpha\beta}(\mathbf{r})$ is the exchange-correlation kernel.²⁴ For numerical calculations, some finite basis must be chosen to represent the spatial dependence of functions $\chi^{\alpha\beta}$, $\chi_0^{\alpha\beta}$, and $f_{\text{Hxc}}^{\alpha\beta}$. Subsequently, Eq. (19) can be solved by matrix inversion.

The quantities defined in the previous section were evaluated using both $\chi^{\alpha\beta}$ and $\chi_0^{\alpha\beta}$. In the latter case, we refer to them as 'bare' quantities and denote them by using subscript 0. Note that both $\chi_0^{\alpha\beta}$ and $\chi^{\alpha\beta}$ satisfy the sum rule in Eqs. (15) and (16) with the same LSDA m_{st} .²⁵

Calculations were performed using two different methods. First method (below as I) is based on the real space finite temperature Matsubara technique. In this formalism, one does not evaluate $\chi_0^{\alpha\beta}(\mathbf{r}, \mathbf{r}', \mathbf{q}, \omega)$ from Eq. (18)

since it is computationally demanding due to presence of the summation over unoccupied states that is entangled with the BZ summation. Instead, one considers the Kohn-Sham susceptibility in the Matsubara time domain. This function can be efficiently evaluated in the real space according to

$$\chi_0^{\alpha\beta}(\mathbf{r}, \mathbf{r}', \mathbf{q}, \tau) = \sum_{\mathbf{R}} e^{-i\mathbf{q}\cdot\mathbf{R}} \sum_{\sigma\sigma'} \sigma_{\sigma\sigma'}^{\alpha} \sigma_{\sigma'\sigma}^{\beta} G_{\mathbf{R}}^{\sigma}(\mathbf{r}, \mathbf{r}', \tau) G_{-\mathbf{R}}^{\sigma'}(\mathbf{r}', \mathbf{r}, \beta - \tau). \quad (21)$$

Here, τ is the Matsubara time ($0 \leq \tau \leq \beta$) and $G_{\mathbf{R}}^{\sigma}(\mathbf{r}, \mathbf{r}', \tau)$ is the imaginary-time Kohn-Sham Green's function given by

$$G_{\mathbf{R}}^{\sigma}(\mathbf{r}, \mathbf{r}', \tau) = - \sum_{n\mathbf{k}} f_{n\mathbf{k}}^{\sigma} \psi_{n\mathbf{k}}^{\sigma}(\mathbf{r}) \psi_{n\mathbf{k}}^{\sigma*}(\mathbf{r}') e^{i\mathbf{k}\cdot\mathbf{R}} e^{\epsilon_{n\mathbf{k}}^{\sigma} \tau / \hbar}. \quad (22)$$

Then, the Kohn-Sham susceptibility is transformed into the Matsubara frequency domain [$\chi_0^{\alpha\beta}(\mathbf{r}, \mathbf{r}', \mathbf{q}, i\omega_k)$ with $\omega_k = \frac{2\pi k}{\hbar\beta}$ being a bosonic Matsubara frequency and k being an integer] according to the prescription from Ref. 26. Subsequently, the enhanced susceptibility in Matsubara frequency domain was found from Eq. (19).

The calculations were based on the full-potential linear augmented plane waves (FLAPW) method as implemented in our in-house electronic structure code.²⁷ The spatial dependence of the susceptibility functions is represented using the mixed product basis set that consists of numerical functions inside the muffin-tin spheres and plane/dual-plane waves in the interstitial region.²⁸ The specific expressions for $\chi_0^{\alpha\beta}(\mathbf{r}, \mathbf{r}', \mathbf{q}, \tau)$ in the product basis are analogous to those used for calculations of the polarizability in Ref. 26.

The Matsubara time real space formalism allows for very efficient susceptibility calculations. In addition, the frequency integrals up to infinity [e.g., Eqs. (11) and (12)] can be very accurately evaluated on the imaginary frequency axis using the contour technique. Therefore, this an ideal method for proper study of FDT. The real frequency axis (with a small imaginary part $\eta=1$ meV) results need to be obtained by analytical continuation. We employ an analytical continuation based on the continued fraction expansion method.²⁹ It is designed to obtain an accurate representation of the low-energy spectrum but may become unstable at higher energies. Therefore, it is important to check the results of our calculations against an alternative approach.

For this reason the most important results were recalculated using the second method (below as II). In this approach the susceptibility is found using the technique implemented in the FLAPW ELK code.³⁰ Here, $\chi_0^{\alpha\beta}(\mathbf{r}, \mathbf{r}', \mathbf{q}, \omega)$ is evaluated directly from Eq. (18) and

the spatial dependence of the susceptibility functions is represented using the plane wave basis. Since it works on the real frequency axis (with a small imaginary part), II does not involve analytical continuation. However, it is difficult to converge the results especially at high energies. In addition, a lot of plane waves are needed to obtain an accurate description of the spatial dependence. Consequently, II is significantly more computationally expensive than I.

C. Computational Details

We consider Fe (bcc), Co (fcc), and Ni (fcc) 3d ferromagnets with experimental lattice parameters. A $16 \times 16 \times 16$ k-point mesh was used.

For I, $T=300$ K and we used 158 nonuniformly distributed (see Ref. 26 for details) mesh points on the imaginary Matsubara time axis. The mixed product basis set was constructed using the interstitial energy cutoff 16.5 Ry and the muffin-tin angular momentum cutoff $L_{\max}^{\text{PB}} = 4$.

For II, the G vector cutoff for the plane wave basis was set to 9.6 \AA^{-1} . For the bare susceptibility calculations, all unoccupied states up to 3.2 Ry above the Fermi energy were included.

For both methods, we ensured that the results are well converged with respect to the computational parameters.

III. RESULTS AND DISCUSSION

A. Small wavevector SDF

Let us first consider SDF for small wavevectors. Fig. 1 (top) shows the transverse spectral function for a fixed low magnitude \mathbf{q} as a function of the frequency for Fe, Co, and Ni calculated using I. For all materials, $A_0^{+-}(\mathbf{q}, \omega)$ has a well defined peak below 0.1 eV. As we increase the number of 3d electrons moving from Fe to Co and then to Ni, the amplitude of the peak decreases and its width increases. The peaks correspond to the collective spin wave excitations because the 'bare' spectral function (Fig. 1) that describes single-particle spin-flip Stoner excitations is very small (below 0.1 eV). Nevertheless, $A_0^{+-}(\mathbf{q}, \omega)$ is nonzero in this low energy region and is responsible for the finite width of the spin wave peaks. While it is not explicitly seen in the figure, the $A_0^{+-}(\mathbf{q}, \omega)$ weight in the low energy region increases with the number of 3d electrons and leads to the corresponding increase of the width of the spin wave peaks. This is in agreement with previous studies.¹⁰ However, $A_0^{+-}(\mathbf{q}, \omega)$ also has a nontrivial structure at higher energies. In particular, we observe a broad maximum at

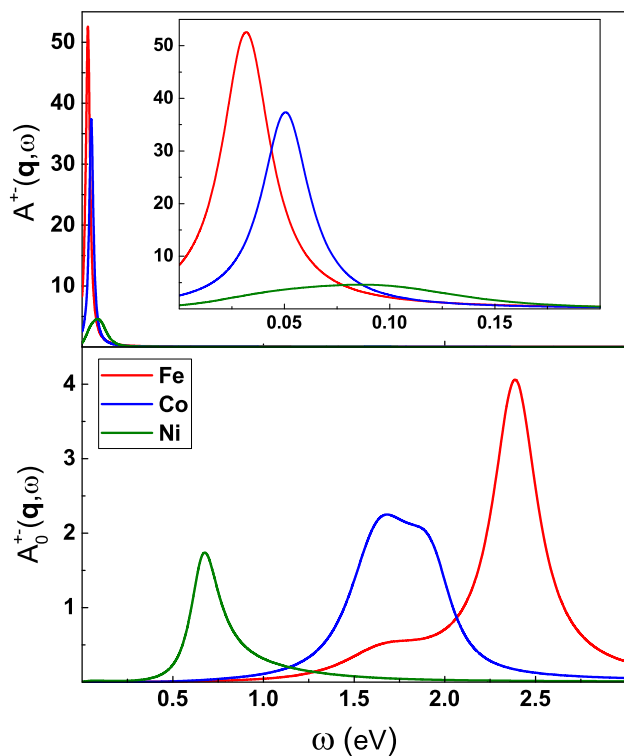


FIG. 1. Small wavevector transverse SDF for Fe, Co, and Ni calculated using I. Top: transverse spectral function. The inset shows the low-energy part of the plot. Bottom: 'bare' transverse spectral function. We used $\mathbf{q} = (0, 0, 0.125)2\pi/a$. Vertical axis units are \hbar^2/eV .

2.5 eV, 1.75 eV, and 0.75 eV for Ni, Co, and Fe, respectively. Interestingly, $A^{+-}(\mathbf{q}, \omega)$ is essentially zero at high energies (above 0.5 eV). This indicates that many-body correlations suppress the high-energy single particle Stoner excitations and instead produce collective spin wave modes.

The low \mathbf{q} longitudinal spectral functions calculated using I is shown in Fig. 2. For all materials $A^{zz}(\mathbf{q}, \omega)$ (Fig. 2 top) has a broad peak structure that slowly decays with energy. The 'bare' longitudinal spectral function (Fig. 2 bottom) has the majority of weight in the same energy range as $A^{zz}(\mathbf{q}, \omega)$ with only a slightly lower amplitude. Since $A_0^{zz}(\mathbf{q}, \omega)$ describes single particle electronic excitations within the same spin channel, we can conclude that the low \mathbf{q} longitudinal SDF originate predominantly from the spin-conserving single-particle electronic excitations. However, the overall magnitude of $A^{zz}(\mathbf{q}, \omega)$ is substantially smaller from $A^{+-}(\mathbf{q}, \omega)$. This indicates that for small \mathbf{q} values the longitudinal SDF can be neglected and only transverse SDF play an important role.

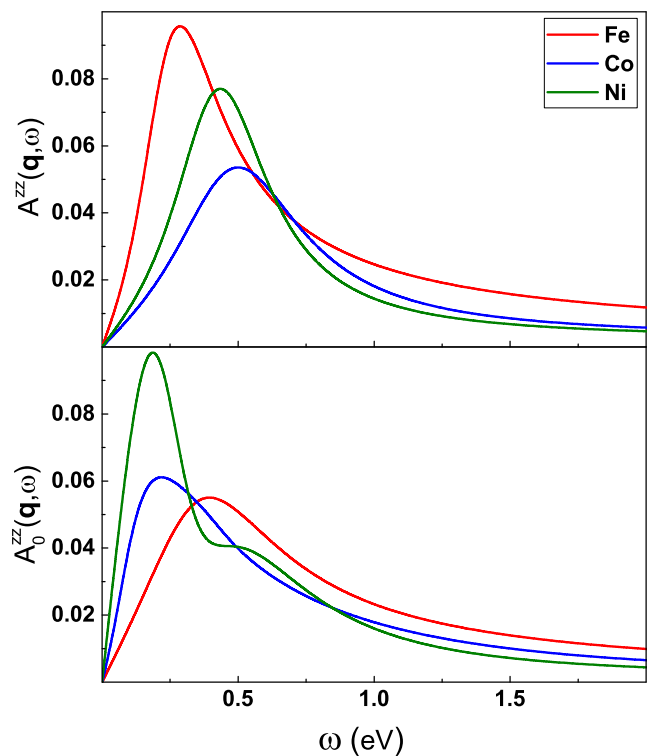


FIG. 2. Small wavevector longitudinal SDF for Fe, Co, and Ni calculated using I. Top: longitudinal spectral function. Bottom: 'bare' longitudinal spectral function. We used $\mathbf{q} = (0, 0, 0.125)2\pi/a$. Vertical axis units are \hbar^2/eV .

B. Density of SDF

Information about spin excitations for other wavevectors can be obtained by analyzing the density of SDF. According to Eq. (6), this function includes SDF from the entire BZ. We focus on transverse SDF. Fig. 3 shows $N^{+-}(\omega)$ and $N_0^{+-}(\omega)$ for all considered materials calculated using I. The same quantities but calculated using the II are shown in Fig. 4. For all materials, both methods produce similar $N^{+-}(\omega)$ curves. In the case of $N_0^{+-}(\omega)$ overall, we also have a reasonable agreement, although for $\omega > 3.5$ eV, we observe some deviation. This is the energy region where the adopted analytical continuation procedure may be inaccurate.

We find that most of the $N^{+-}(\omega)$ weight exists for $\omega < 1$ eV. On the other hand, $N_0^{+-}(\omega)$ (that describes the spectrum of single-particle Stoner excitations) is much smaller in this energy range but instead it extends to much higher energies with the majority of the spectrum residing up to an energy of the order of the $3d$ electronic bandwidth ($W_{el} \simeq 5-6$ eV). Therefore, similarly as in the case of small \mathbf{q} SDF, we conclude that many-body interactions suppress the high-energy Stoner excitations

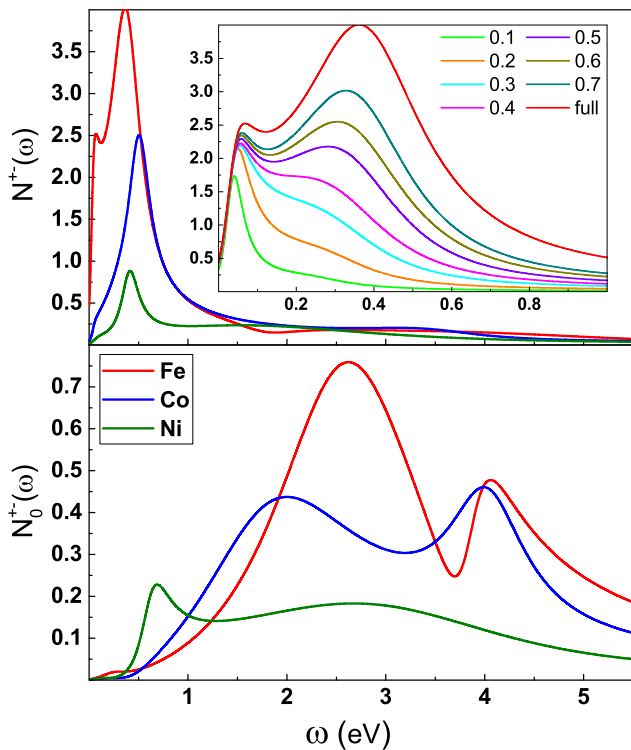


FIG. 3. On-site transverse SDF spectrum for Fe, Co, Ni calculated using I. Top: density of transverse SDF. The inset shows the low energy part of the plot for Fe (the red curve denoted as 'full') compared with the partial- \mathbf{q} density of transverse SDF [see Eq. (7), different curves are denoted by the value of the $\Omega_{\mathbf{q}}/\Omega_{\text{BZ}}$ ratio]. Bottom: 'bare' density of transverse SDF. Vertical axis units are \hbar^2/eV .

and transform them into low-energy collective modes.

For Fe, $N^{+-}(\omega)$ has a two-peak structure with the smaller narrow low-energy peak at 50 meV and the larger broad high-energy peak at 0.4 eV. While for Co and Ni only the high-energy peak can be clearly seen, for both materials we can also identify a low-energy shoulder at ~ 50 meV. This indicates that the two-peak structure is a generic feature for the $3d$ magnets. We emphasize that the shape of $N^{+-}(\omega)$ is, thus, distinctly different from the single-peak structure of the spectral function. This indicates that transverse excitations with large wavevectors play an important role. This point is quantitatively illustrated in the inset of Fig. 3 in the case of Fe. Here, the partial- \mathbf{q} density of transverse SDF, Eq. (7), is shown for different values of the $\Omega_{\mathbf{q}}/\Omega_{\text{BZ}}$ ratio. As seen, for $\omega < 0.1$ eV, SDF with a small \mathbf{q} that correspond to traditional spin wave excitations are dominant and they are responsible for the low-energy peak. For higher energies, however, SDF with a large \mathbf{q} are crucial. In particular, the large high-energy peak originates

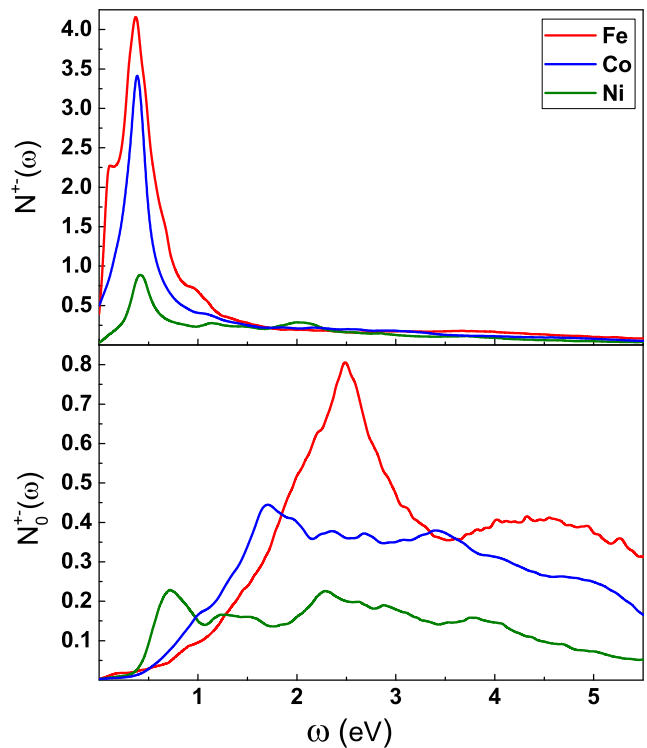


FIG. 4. On-site transverse SDF spectrum for Fe, Co, Ni calculated using II. Top: density of transverse SDF. Bottom: 'bare' density of transverse SDF. Vertical axis units are \hbar^2/eV .

exclusively from collective excitations with large \mathbf{q} values that are localized in the real space. Analysis of $N_{\Omega_{\mathbf{q}}}^{+-}(\omega)$ for Co and Ni shows that the origin of the two-peak structure is similar for all considered systems.

The above discussion indicates that in order to properly include SDF in calculations of ground state and thermodynamic properties, one needs to take into account excitations for all \mathbf{q} . Therefore, restriction to SDF from only limited parts of the BZ (for instance the long wave approximation commonly used in spin fluctuation theories or the DMFT single-site approximation) can lead to an inaccurate material description and misleading results.

C. Static magnetic moment sum rule

Let us now consider the static magnetic moment sum rule Eq. (15) which relates the transverse SDF spectrum to the LDA static magnetic moment. Fig. 5 shows $m_{\text{st}}(\omega)$ evaluated from both $\chi^{\alpha\beta}$ and $\chi_0^{\alpha\beta}$. The same plot but obtained using II is shown in Fig. 6. As seen, the sum rule is almost perfectly satisfied in both sets of cal-

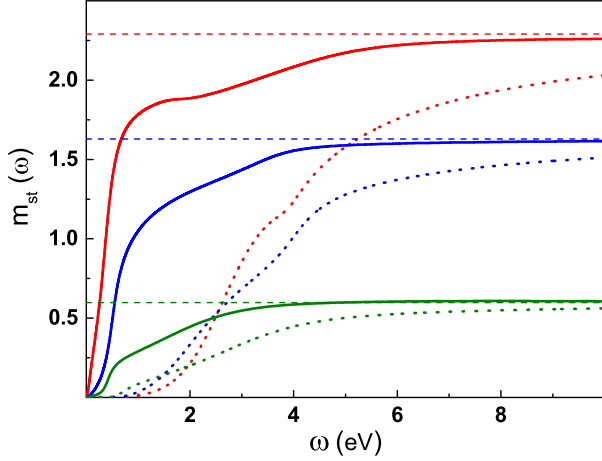


FIG. 5. Static magnetic moment sum rule (see Eq. (5)) evaluated using I. Red, blue, and green curves correspond to Fe, Co and Ni, respectively. Horizontal dashed lines denote the LDA value of the static magnetic moment. Full and dotted line denote $m_{\text{st}}(\omega)$ and $m_{\text{st},0}(\omega)$, respectively. Vertical axis units are μ_B .

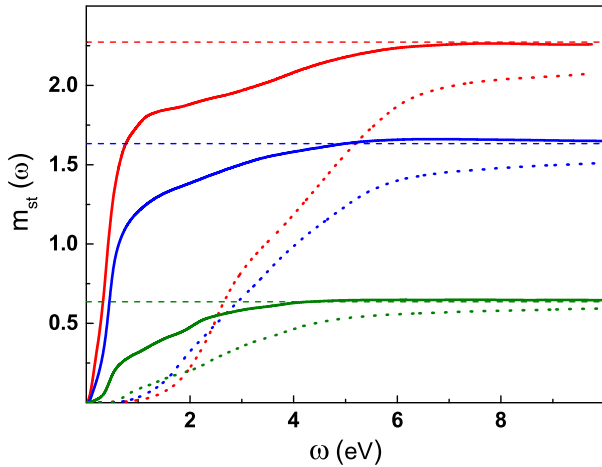


FIG. 6. Static magnetic moment sum rule (see Eq. (5)) evaluated using II. Red, blue, and green curves correspond to Fe, Co and Ni, respectively. Horizontal dashed lines denote the LDA value of the static magnetic moment. Full and dotted line denote $m_{\text{st}}(\omega)$ and $m_{\text{st},0}(\omega)$, respectively. Vertical axis units are μ_B .

culations. The shapes of the $m_{\text{st}}(\omega)$ curves are also very similar in both methods (even at high energies). This is true especially for the enhanced susceptibility. This indicates that overall the analytical continuation is quite reliable.

For Fe, the LSDA value of the static local moment is

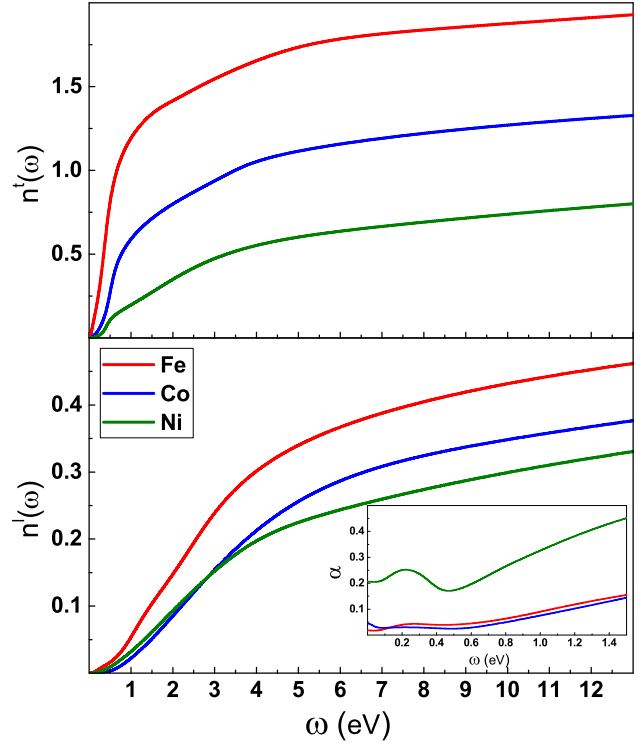


FIG. 7. Energy dependence of number of on-site transverse SDF for Fe, Co, and Ni calculated using I. Top: number of on-site transverse SDF. Bottom: 'bare' number of on-site transverse SDF. Vertical axis units are \hbar^2 . The inset shows the energy dependence of the adiabaticity parameter α defined as twice the ratio of $n^l(\omega)$ to $n^t(\omega)$.

obtained with the inclusion of transverse excitations up to energy W_{el} . On the other hand, for the 'bare' SDF spectrum, energies up to 13 eV are required to obtain a similar level of accuracy. In the case of system with smaller moment (like Ni and Co) such convergence is obtained for lower energies.

D. Number of SDF

The number of transverse SDF calculated using I is shown in Fig. 7 as a function of energy for different ferromagnetic metals. As expected from the above analysis of $N^{+-}(\omega)$, the most of transverse SDF exist for $\omega < 1$ eV with the high-energy peak providing the major contribution. Nevertheless, for $\omega > 1$ eV, $n^t(\omega)$ still shows a sizable increase up to $\omega \sim W_{\text{el}}$. For $\omega > W_{\text{el}}$, only a slow increase of $n^t(\omega)$ is observed that corresponds to excitations involving semicore and/or high-energy unoccupied states.

The number of longitudinal SDF is shown in Fig. 7

(bottom). As seen, longitudinal SDF exist at all energies with the majority of the spectrum being accumulated for $\omega < W_{\text{el}}$. While at low energies ($\omega < 1$ eV) $n^l(\omega)$ is much smaller than $n^t(\omega)$, for $\omega \sim W_{\text{el}}$ both functions have the same order of magnitude. Thus, our study naturally addresses the validity of adiabatic approximation³¹ in spin dynamics. In all studied materials longitudinal SDF can be neglected at least up to 1 eV energy range and pure transversal spin dynamics is valid. The important difference with a spin dynamics in magnetic insulators is a presence strong non spin wave transversal SDF of itinerant nature.

We emphasize that both for transverse and longitudinal SDF, the majority of excitations lie at energies much higher than those accessible from inelastic neutron scattering experiments. Therefore, different experimental techniques (high-energy spin resolved spectroscopies³²) are required to probe the full spectrum. Both $n^t(\omega)$ and $n^l(\omega)$ are continuous steadily increasing functions of energy and therefore, it is not possible to rigorously introduce any energy cutoff when including SDF in studies of metals. Thus, with a temperature increase for instance, more SDF are excited and contribute to the magnetic properties of the itinerant metal. This feature is in stark contrast with the traditional magnetic insulator picture where excitations for energies above the spin wave spectrum do not exist and *all* SDF are excited at corresponding temperatures.

E. FDT

In this section we study FDT using I that allows for an efficient evaluation of the infinite energy integrals. In particular, FDT can be used to obtain the effective fluctuating moment $m_{\text{eff}}(\omega)$. This quantity provides a useful measure of the strength of SDF at a given energy since it can be compared with static moment values in magnetic materials. Note that $m_{\text{eff}}(\omega)$ is directly related to SC through Eqs. (13) and (14). Since the main contribution to SC arises from the spin zero-point motion SDF (except when $\omega < 1/\beta$ where thermal SDF are important), the energy dependence of $m_{\text{eff}}^{t,l}(\omega)$ follows roughly the square root of $n^{t,l}(\omega)$. Therefore, $m_{\text{eff}}(\omega)$ is an ever increasing smooth function of energy. For this reason, it is sufficient to provide $m_{\text{eff}}(\omega)$ at several characteristic energy scales, see Table I. Here, the values of $m_{\text{eff}}(\omega)$ as well as $m_{\text{eff}}^t(\omega)$ and $m_{\text{eff}}^l(\omega)$ calculated both from $\chi^{\alpha\beta}$ and $\chi_0^{\alpha\beta}$ using I are shown. At low energies ($\omega \simeq 0.1$ eV), $m_{\text{eff}}(\omega)$ originates mainly from traditional long-wavelength spin waves (low-energy peak in top panel of Fig. 3) and it is much smaller than the static magnetic moment. For $\omega \simeq 1$ eV, the main part of the SDF spectrum that consists of localized in real space large \mathbf{q} collective transverse

TABLE I. Effective fluctuating moment (in units of μ_B) calculated using I at different energies for all considered materials. The zero values correspond to the calculated values that are less than $0.1 \mu_B$.

ω (eV)	0.1	1	5	12	∞
Fe: $m_{\text{eff}}^t(\omega)$	0.8	2.2	2.7	2.8	3.1
$m_{\text{eff},0}^t(\omega)$	0.0	0.3	1.8	2.2	2.6
$m_{\text{eff}}^l(\omega)$	0.1	0.5	1.2	1.3	1.6
$m_{\text{eff},0}^l(\omega)$	0.0	0.2	1.1	1.2	1.5
$m_{\text{eff}}(\omega)$	0.8	2.3	2.9	3.1	3.5
$m_{\text{eff},0}(\omega)$	0.0	0.4	2.1	2.5	3.1
Co: $m_{\text{eff}}^t(\omega)$	0.2	1.5	2.1	2.3	2.7
$m_{\text{eff},0}^t(\omega)$	0.0	0.3	1.7	2.0	2.4
$m_{\text{eff}}^l(\omega)$	0.0	0.3	1.0	1.2	1.5
$m_{\text{eff},0}^l(\omega)$	0.1	0.3	1.0	1.2	1.5
$m_{\text{eff}}(\omega)$	0.2	1.6	2.3	2.6	3.1
$m_{\text{eff},0}(\omega)$	0.1	0.5	2.0	2.3	2.9
Ni: $m_{\text{eff}}^t(\omega)$	0.1	0.9	1.6	1.8	2.2
$m_{\text{eff},0}^t(\omega)$	0.0	0.5	1.3	1.6	2.1
$m_{\text{eff}}^l(\omega)$	0.0	0.4	0.9	1.1	1.5
$m_{\text{eff},0}^l(\omega)$	0.1	0.3	0.9	1.1	1.4
$m_{\text{eff}}(\omega)$	0.1	1.0	1.8	2.1	2.7
$m_{\text{eff},0}(\omega)$	0.1	0.6	1.6	1.9	2.0

excitations (high-energy peak in top panel of Fig. 3) is also included and $m_{\text{eff}}(\omega)$ becomes comparable to m_{st} . A further energy increase up to $\omega \simeq W_{\text{el}}$ includes all excitations within the $3d$ band and $m_{\text{eff}}(\omega)$ is increase by 20-70%. A large part of this enhancement originates from longitudinal SDF. For higher energies, only a slow increase of m_{st} is observed. However, this accumulates to a significant contribution for $\omega = \infty$.

In Fig. 8 we plot $m_{\text{eff}} \equiv m_{\text{eff}}(\omega = \infty)$ as a function of the number of $3d$ electrons. In addition to the considered materials, we also included the data for $3d$ paramagnetic metals from Ref. 22. As seen, m_{eff} has a value of several μ_B for all metals. Interestingly, the value of m_{eff} seems to be independent on the presence of a magnetic order, but it is rather determined by the $3d$ band population. Indeed, the dependence of m_{eff} on the $3d$ electron number is reminiscent of the Slater Pauling curve. Below the half-filling, m_{eff} increases with the $3d$ electron number. Above the half-filling, however, an opposite trend is observed. Two mechanisms that are similar in strength but differ in origin are responsible for such behavior. First, as indicated by the blue curve in Fig. 8, the number of Stoner single particle excitations within the $3d$ band is maximized at half-filling. Second, the many body enhancement due to electronic correlations is also strongest for a half-filled band.

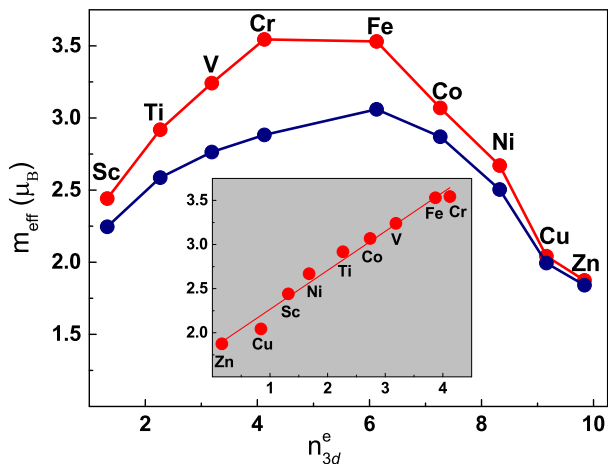


FIG. 8. The full effective fluctuating magnetic moment (m_{eff}) calculated using I as a function of the the number of 3d electrons (red). The blue curve denotes the 'bare' m_{eff} evaluated using the Kohn-Sham susceptibility. The inset shows m_{eff} as a function of $n_{3d} = \min(n_{3d}^e, n_{3d}^h)$, where n_{3d}^e and n_{3d}^h is the number of 3d electrons and holes, respectively. The line in the inset is the linear fit of the data.

In the inset of Fig. 8, we show m_{eff} as a function of the number of 3d carriers as $n_{3d} = \min(n_{3d}^e, n_{3d}^h)$. Here, n_{3d}^e and n_{3d}^h is the number of 3d electrons and holes, respectively. We find that m_{eff} shows approximately a linear dependence on n_{3d} . The fitting to a linear function results in the following empirical formula:

$$m_{\text{eff}} \approx 0.4n_{3d} + 1.8. \quad (23)$$

Note that the same equation was obtained in Ref. 22 using only 3d paramagnets. This indicates that every 3d electron or hole contributes approximately the moment of $0.4\mu_B$ to m_{eff} . The nonzero intercept corresponds to m_{eff} for a completely filled or completely empty 3d band. It originates from electronic transitions involving semi-core levels and high-energy unoccupied states.

As seen in Fig. 8 the $m_{\text{eff},0}$ that originate purely from single particle excitations is also appreciable. This fact is of crucial importance since it is the difference between m_{eff} and the $m_{\text{eff},0}$ that determines the effect of SDF on ground state and thermodynamic properties of materials. Indeed, the measure of the SDF correlation energy is provided by $\Delta n^{t,l}(\omega) = n^{t,l}(\omega) - n_0^{t,l}(\omega)$ (see, for instance, the recent review Ref. 33). The energy dependence of these quantities for Fe, Co, and Ni is shown in Fig. 9. As seen, $\Delta n^t(\omega)$ converges for energies of the order of W_{el} and reaches a value corresponding to a moment of $1.7\mu_B$, $1.1\mu_B$, and $0.8\mu_B$ for Fe, Co, and Ni, respectively. The SDF correlation energy can be then

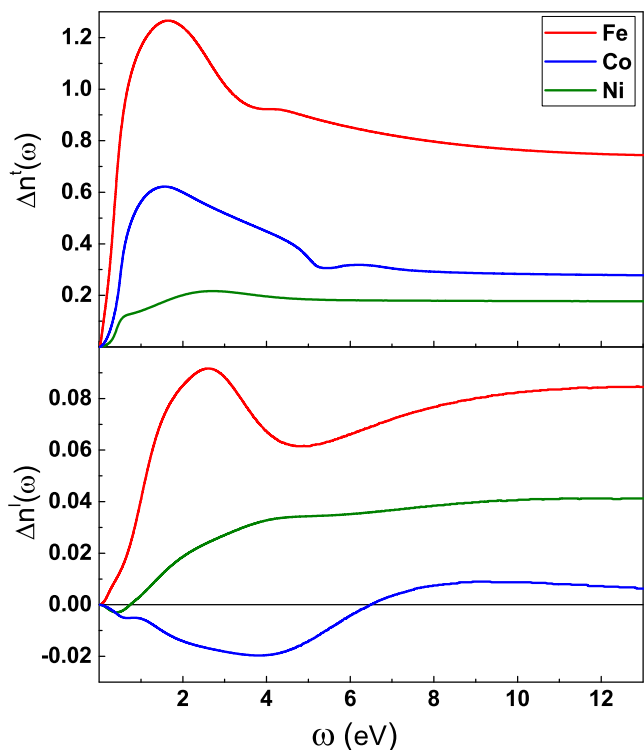


FIG. 9. Difference between the number and the 'bare' number of transverse (top) and longitudinal (bottom) SDF calculated using I. Vertical axis units are \hbar^2 .

roughly estimated as a typical energy required to form such magnetic moments. Clearly, the SDF correlation energy is significant and, therefore, SDF corresponding to this $\Delta n^t(\omega)$ should be explicitly included in electronic structure calculations and all energies up to W_{el} should be treated on equal footing. For Fe and Co, $\Delta n^l(\omega)$ is less than 10% of $\Delta n^t(\omega)$ and can therefore be neglected. On the other hand, for Ni, $\Delta n^l(\omega)$ plays a more significant role and should be included.

Finally, let us discuss the behavior of the moment deviation square as defined in Eq. (17). An energy independent version of this quantity is often used in spin fluctuations models.³ Fig. 10 shows the energy dependence of $\langle \delta m^2 \rangle(\omega)$ calculated using I. For Fe, $\langle \delta m^2 \rangle(\omega)$ rapidly increases with energy until an inflection point at $\omega \sim 0.5$ eV, where it reaches a value of about $1.5\mu_B^2$. For larger energies, $\langle \delta m^2 \rangle(\omega)$ still shows a significant increase and at $\omega = 3$ eV, it is roughly equal to $4.5\mu_B^2$. For larger energies yet, only a slow increase of $\langle \delta m^2 \rangle(\omega)$ is observed. For Co and Ni, the energy dependence of $\langle \delta m^2 \rangle(\omega)$ is identical while $\omega > 4$ eV. For lower energies, $\langle \delta m^2 \rangle(\omega)$ is larger for Co. In particular, at $\omega = 0.5$ eV, $\langle \delta m^2 \rangle(\omega)$ is roughly equal to $1\mu_B^2$ and $0.5\mu_B^2$ for Co and Ni, respectively. We point out that at any energy,

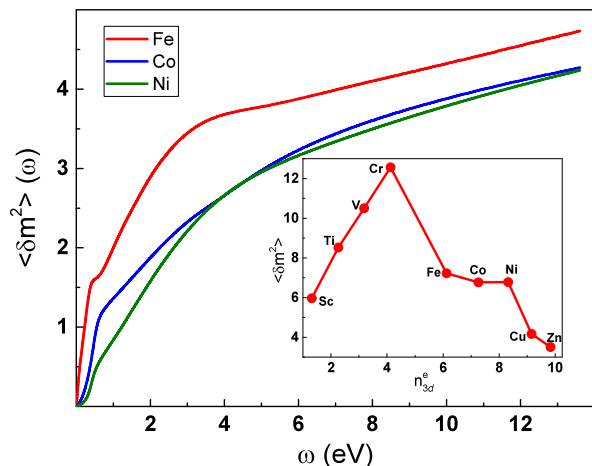


FIG. 10. Energy dependence of the moment deviation square as calculated using I. The inset shows $\langle \delta m^2 \rangle \equiv \langle \delta m^2 \rangle(\omega \rightarrow \infty)$ as a function of the the number of 3d electrons. The vertical axis units are μ_B^2 .

the relative importance of $\langle \delta m^2 \rangle(\omega)$ with respect to the static moment is the largest for Ni. Therefore, SDF in Ni are expected to play a particularly important role.

The inset of Fig. 10 shows $\langle \delta m^2 \rangle \equiv \langle \delta m^2 \rangle(\omega \rightarrow \infty)$ as a function of the the number of 3d electrons. Interestingly, Fe, Co, and Ni all have a $\langle \delta m^2 \rangle$ value close to $7 \mu_B^2$. We also included the data for 3d paramagnets from Ref. 22. In this case, $\langle \delta m^2 \rangle$ is equal to the square of m_{eff} (the static moment is zero). Unlike m_{eff} , $\langle \delta m^2 \rangle$ does not have a smooth dependence of the 3d band population. In particular, $\langle \delta m^2 \rangle$ is significantly diminished when the ferromagnetism sets in. This indicates that the spin fluctuations of the 3d electrons that participate in the formation of the static magnetic moment are (at least partially) reduced.

IV. CONCLUSIONS

SDF in 3d ferromagnetic metals were analyzed using first principles electronic structure calculations of the dynamic spin susceptibility tensor. The accuracy of the results were carefully tested by using two inde-

pendent calculation methods. We showed that the SDF are spread continuously over the entire BZ as well as the wide energy range extending far above energies accessible in neutron scattering experiments. Thus, no well-defined wavevector and frequency cutoffs (as often assumed) can be reliably introduced in such materials. In particular, we show that for the correct description of the SDF correlation energy all excitations below energy of the order of 3d electronic bandwidth should be included on equal footing without usage of any long wavelength or atomistic approximations. In addition, our analysis of different polarizations of susceptibility tensor demonstrated that the adiabatic approximation is well justified and spin dynamics in these materials has nearly pure transversal character at least up to 1 eV energy range.

Consequently, a major result of fluctuation theory, fluctuation-dissipation theorem, has been carefully evaluated using a complete spectrum of SDF. It was shown that FDT in 3d ferromagnets has two main constituents. One, at low energies (for instance, for Fe at ~ 50 meV) is a minor contribution due to traditional low- \mathbf{q} spin wave excitations, while the second, much larger high-energy (for instance for Fe at ~ 0.4 eV) component, corresponds to localized in real space large wavevector collective spin excitations. Such two-component structure is observed for all considered materials and we believe this is a rather generic feature of magnetic metals.

Overall, the total effective fluctuating moment from itinerant electrons is on the order of several Bohr magnetons with a significant contribution at low energies. A unique linear dependence of the effective fluctuating moment on electronic population has been found.

ACKNOWLEDGMENTS

This work was supported by the Critical Materials Institute, an Energy Innovation Hub funded by the U.S. Department of Energy (DOE). V. P. acknowledges the support from the Office of Basic Energy Science, Division of Materials Science and Engineering. V.N. and A.I. acknowledge the support from the Hamburg Centre for Ultrafast Imaging (CUI). The research was partially performed at Ames Laboratory, which is operated for the U.S. DOE by Iowa State University under contract # DE-AC02-07CH11358.

* alexwysoki2@gmail.com

† Present address: Department of Physics and Astronomy, Rutgers University, Piscataway, New Jersey 08856, USA

¹ T. Moriya, *Spin fluctuations in itinerant electron magnetism* (Springer, Berlin, 1985).

² Y. Takahashi, *Spin Fluctuation Theory of Itinerant Electron Magnetism* (Springer, New York, 2013).

³ *Itinerant Electron Magnetism: Fluctuation Effects*, Eds. D. Wagner, W. Brauneck, and A. Solontsov, (Kluwer Academic Publishers, Dordrecht, 1998).

- ⁴ D. J. Kim, *New Perspectives in Magnetism of Metals* (Kluwer Academic/Plenum Publishers, New York, 1999).
- ⁵ M. Brando, D. Belitz, F.M. Grosche, and T.R. Kirkpatrick, *Rev. Mod. Phys.* **88**, 025006 (2016).
- ⁶ R. Kubo, *Rep. Prog. Phys.* **29**, 255 (1966).
- ⁷ P. Dai, *Rev. Mod. Phys.* **87**, 855 (2015).
- ⁸ *Ultrafast Magnetism I*, Eds. J-Y. Bigot, W. Hübner, T. Rasing, and R. Chantrell, (Springer, Berlin, 2013).
- ⁹ S. Y. Savrasov, *Phys. Rev. Lett.* **81**, 2570 (1998).
- ¹⁰ P. Buczek, A. Ernst, and L. M. Sandratskii, *Phys. Rev. B* **84**, 174418 (2011).
- ¹¹ B. Rousseau, A. Eiguren, and A. Bergara, *Phys. Rev. B* **85**, 054305 (2012).
- ¹² S. Lounis, M. dos Santos Dias, and B. Schweglinghaus, *Phys. Rev. B* **91**, 104420 (2015).
- ¹³ T. Kotani and M. van Schilfhaarde, *J. Phys.: Condens. Matter* **20**, 295214 (2008).
- ¹⁴ E. Şaşıoğlu, A. Schindlmayr, C. Friedrich, F. Freimuth, and S. Blügel, *Phys. Rev. B* **81**, 054434 (2010).
- ¹⁵ M. Shimizu, *J. Magn. Magn. Mat.* **31**, 299 (1983).
- ¹⁶ G. G. Lonzarich, *J. Magn. Magn. Mat.* **70**, 20 (1987).
- ¹⁷ A. Z. Solontsov and D. Wagner, *Phys. Rev. B* **51**, 12410 (1995).
- ¹⁸ A. Solontsov and V. P. Antropov, *Phys. Rev. B* **81**, 214402 (2010).
- ¹⁹ V. P. Antropov and A. Solontsov *J. Appl. Phys.* **109**, 07E116 (2011).
- ²⁰ G. Kotliar, S. Y. Savrasov, K. Haule, V. S. Oudovenko, O. Parcollet, and C. A. Marianetti, *Rev. Mod. Phys.* **78**, 865 (2006).
- ²¹ N. E. Zein and V. P. Antropov, *Phys. Rev. Lett.* **89**, 126402 (2002).
- ²² A. L. Wysocki, A. Kutepov, and V. P. Antropov, *Phys. Rev. B* **94**, 140405(R) (2016).
- ²³ J. Callaway and C. S. Wang, *J. Phys. F* **5**, 3119 (1975).
- ²⁴ E. K. U. Gross and W. Kohn, *Phys. Rev. Lett.* **55**, 2850 (1985).
- ²⁵ D. M. Edwards and M. A. Rahman, *J. Phys. F: Metal Phys.* **8**, 1501 (1978).
- ²⁶ A. Kutepov, K. Haule, S. Y. Savrasov, and G. Kotliar, *Phys. Rev. B* **85**, 155129 (2012).
- ²⁷ A. L. Kutepov and S. G. Kutepova, *J. Phys.: Condens. Matter* **15**, 2607 (2003).
- ²⁸ F. Aryasetiawan and O. Gunnarsson, *Phys. Rev. B*, **49**, 7219 (1994).
- ²⁹ H. J. Vidberg and J. W. Serene, *J. Low Temp. Phys.* **29**, 179 (1977).
- ³⁰ <http://elk.sourceforge.net/>
- ³¹ V. P. Antropov, M. I. Katsnelson, B. N. Harmon, M. van Schilfhaarde, and D. Kusnezov, *Phys. Rev. B*, **54**, 1019 (1996).
- ³² *Polarized electrons in surface physics*, Eds. R. Feder (World Scientific, Singapore, 1985).
- ³³ J. F. Dobson and T. Gould, *J. Phys.: Condens. Matter* **24**, 073201 (2012).